Research Square

Preprints are preliminary reports that have not undergone peer review.
They should not be considered conclusive, used to inform clinical practice,
or referenced by the media as validated information.

Influence of Fe Doping on the Structural, Electrical, and Room-Temperature Ethanol Sensing Properties of Sol–Gel Spin-Coated TiO_2 Thin Films

Neha Sharma
Kanya Maha Vidyalaya
Rajesh Kumar
rajesh.12236@lpu.co.in

Lovely Professional University

Article

Keywords: Fe-doped TiO_2 thin films, Sol–gel spin coating, Ethanol gas sensor, Room-temperature sensing, Oxygen vacancies, Electrical conductivity, Selectivity, Long-term stability

Posted Date: August 25th, 2026

DOI: https://doi.org/10.21203/rs.3.rs-10609073/v1

License: This work is licensed under a Creative Commons Attribution 4.0 International License.
Read Full License

Additional Declarations: No competing interests reported.

Influence of Fe Doping on the Structural, Electrical, and Room-Temperature Ethanol Sensing Properties of Sol–Gel Spin-Coated TiO_2 Thin Films

Neha Sharma[a], Rajesh Kumar[b]*

[a]*Department of Physics, Kanya Maha Vidyalaya, Jalandhar (Punjab), 144001, India*

[b]*School of Chemical Engineering and Physical Science, Lovely Professional University, Phagwara (Punjab)-144411, India*

Corresponding author *rajesh.12236@lpu.co.in

Abstract

Using the sol–gel spin-coating process, pure and Fe-doped TiO_2 thin films were effectively created on glass substrates to study the ethanol-sensing behavior at room temperature. This technique made it possible to create consistent, well-adhered films, which offered a good platform for researching how Fe^{3+} doping affected their structural, electrical, and sensing properties. It was discovered that adding Fe ions to the TiO_2 lattice greatly altered the microstructure and improved the films' charge transport characteristics. The introduction of defect states and a rise in the concentration of oxygen vacancies, which are essential for gas-sensing processes, are responsible for these advances. The TiO_2 thin film with 0.5% Fe showed the most promising sensing ability toward ethanol vapors at ambient temperature among the several doping doses investigated. The 0.5% Fe-doped TiO_2 film showed a high sensor response of 19.54 when exposed to 500 ppm of ethanol, which was much greater than that of the undoped and other doped samples. The optimal balance between surface active sites and electrical conductivity attained at this specific doping level is probably the cause of this improved response. Furthermore, during several testing cycles, no deterioration in the sensor response was noted, and the stability of the sensing features was assessed. This suggests that the Fe-doped TiO_2 thin films have dependable sensing capability and good durability. Overall, the study demonstrates that controlled Fe doping is a successful method for enhancing the ethanol-sensing capacity of TiO_2 thin films at ambient temperature.

Keywords: Fe-doped TiO_2 thin films; Sol–gel spin coating; Ethanol gas sensor; Room-temperature sensing; Oxygen vacancies; Electrical conductivity; Selectivity; Long-term stability.

1. Introduction:

In the fields of industrial automation, environmental safety, and medical diagnostics, the precise and quick identification of volatile organic compounds (VOCs) has become crucial. VOCs easily evaporate into the atmosphere from a variety of anthropogenic and biogenic sources because of their high vapour pressure and low boiling temperatures at room temperature. Volatile organic compounds

(VOCs), mostly produced by industrial operations and automobile exhaust, pose substantial hazards to both public health and environmental ecosystems. In addition to significantly increasing the risk of cancer, prolonged exposure to high VOC concentrations can cause acute respiratory irritation, neurological headaches, and serious organ damage to the kidneys and liver. [1][2]. As a ubiquitous volatile organic molecule (VOC), gaseous ethanol is extensively utilised across chemical processes, biomedical sectors, and food preservation applications [3]. However, the accumulation of its vapour poses serious safety risks due to the fact that it is a colourless, extremely combustible, and volatile liquid. Long-term exposure to concentrated ethanol vapours causes acute respiratory and ocular irritation, dizziness, nausea, and severe vomiting, among other urgent physiological problems [4]. The Occupational Safety and Health Administration (OSHA) enforces a stringent permissible exposure limit (PEL) of 1000 parts per million (ppm) for an 8-hour shift in order to reduce these occupational dangers. This regulatory threshold emphasises how crucial it is to create extremely effective, real-time ethanol tracking systems in order to protect the environment and worker health [5]. Consequently, developing ethanol gas sensors characterised by high sensitivity, rapid response/recovery dynamics, and remarkable cross-selectivity is of crucial relevance. Due to its crucial integration into automated quality control monitoring in the beverage and fermentation sectors as well as medical breath analysis for non-invasive health screening, these platforms have attracted significant scientific and commercial attention [6,7]. Metal oxide semiconductors (MOS) have garnered a lot of attention in the creation of gas sensors because of their strong adherence to substrates, high surface reactivity, and superior sensing efficiency. Because of its stability, affordability, and sensitivity to diverse gases, a variety of MOS materials, including TiO_2, ZnO, NiO, CuO, SnO_2, and others, have been used in a wide range of gas sensors [8–12]. Titanium dioxide (TiO_2) is an inherent n-type semiconductor with a broad band gap of about 3.2 eV for the anatase phase and 3.0 eV for the rutile phase. Because of its non-toxicity, high refractive index, remarkable biocompatibility, transparency to visible light, and inexpensive cost of production, it is used extensively [13,14]. Anatase, rutile, and brookite are the three main crystalline polymorphs of TiO_2, each of which has unique structural and electrical characteristics that significantly influence gas-sensing performance. The anatase phase usually provides high baseline gas sensitivity and enhanced surface reactivity due to its large specific surface area and high density of surface flaws [15]. The most thermodynamically stable phase, on the other hand, is rutile, which offers improved electrical conductivity and long-term sensor stability at high operating temperatures. Although brookite's complex production restricts its use on its own, the creation of mixed-phase matrices (such as anatase–rutile homojunctions) frequently produces far better gas-sensing dynamics. Optimised interfacial charge separation and faster electron transport across phase boundaries produce this synergistic improvement, which results in increased sensitivity and quick response/recovery kinetics [16]. For gas-sensing applications, titanium dioxide arranged in thin-film architectures has several advantages over bulk counterparts, mainly because of increased crystallinity, excellent visible-light transparency, and an improved surface-to-volume ratio. These thin-film matrices maximise

surface-active sites available for chemisorption, making them the perfect platform for ethanol detection. Numerous deposition methods, such as chemical vapour deposition (CVD), reactive magnetron sputtering, spray pyrolysis, and sol-gel processing, are frequently used to create these films. Each method offers exact control over grain boundary density, film thickness, and structural phase distribution [17–21]. Pristine TiO_2 thin films often have poor selectivity, low baseline sensitivity, and high operating temperature requirements despite their structural advantages. In order to get around these restrictions, a very successful method of modifying the physical, chemical, optical, and electrical characteristics of metal oxide frameworks is the incorporation of transition metal dopants into the parent oxide lattice. The host band structure, charge-carrier concentrations, and highly active surface defects—like oxygen vacancies—that act as catalytic foci for gas adsorption are all systematically altered by the introduction of transition metal ions. As a result, many scientists have used targeted metal doping to improve chemiresistive sensing platforms, producing encouraging advances in cross-selectivity profiles and response dynamics [22–24]. Even though transition metal-doped TiO_2 has been extensively studied for gas-sensing applications, more research is still needed to fully comprehend how Fe incorporation affects the structural, electrical, and ethanol-sensing properties of sol-gel spin-coated TiO_2 thin films, especially when operating at room temperature. The microstructure and electrical characteristics of TiO_2 can be altered by Fe doping, according to earlier research; nevertheless, the connection between dopant concentration and sensing performance has not been methodically established for this production method. Furthermore, traditional chemiresistive ethanol sensors frequently have poor selectivity when interfering gases are present, low sensitivity at low concentrations, and decreased long-term operational stability. In order to determine the ideal doping level for improved room-temperature ethanol sensing, the current work methodically examines the impact of Fe concentration on the structural, electrical, and gas-sensing characteristics of sol–gel spin-coated TiO_2 thin films. Iron was chosen as the dopant because its ionic radius is similar to that of TiO_2, allowing it to be incorporated into the TiO_2 lattice with little structural distortion and perhaps altering the material's electrical and sensing properties. While Ti^{4+} can replace Ti^{4+} in the crystal lattice, Fe^{3+} has an atomic radius of 0.64Å, whereas Ti^{4+} has an atomic radius of 0.68Å. Furthermore, the band gap of TiO_2 is decreased by the Fe ion's 2.6 eV band gap [25]. The fabrication of Fe-incorporated TiO_2 thin films using a meticulously optimised sol–gel spin-coating method for effective room-temperature ethanol detection is what makes this work novel. An ideal Fe concentration (0.5 at.%) for improved sensing properties was found after a methodical study was conducted to determine the relationship between Fe dopant concentration, structural evolution, electrical transport, and gas-sensing performance. Fe-modified TiO_2 thin films have the potential to be low-power sensing materials for ethanol detection, as demonstrated by the optimised thin film's strong sensor response, quick reaction and recovery, great repeatability, long-term stability, and low humidity interference at room temperature.

2. Experimental Details

2.1. Sol Synthesis and Thin film Fabrication:

TiO_2 thin films were synthesised using titanium (IV) isopropoxide (TTIP, 99.5%, Sigma-Aldrich) as the titanium precursor. The iron dopant precursor was hydrated ferric chloride ($FeCl_3 \cdot xH_2O$), and the solvent was pure ethanol. During the sol production process, diethylene glycol (DEG) was employed as a stabilising agent to control the hydrolysis and condensation reactions. Every chemical utilised was analytical grade and didn't require any additional purification. Sol-gel spin-coating was used to create pure and Fe-doped TiO_2 thin films. First, ethanol and diethylene glycol were combined in a 20:1 volumetric ratio while being continuously stirred magnetically. To create a homogenous precursor sol, 1 mL of titanium (IV) isopropoxide was then gradually added to the mixture while stirring continuously.

Fe concentrations of 0.5, 1.0, 1.5, and 2.0 at.% were obtained for Fe-doped materials by adding the proper amounts of hydrated ferric chloride to the precursor solution. Before deposition, the combined precursor solutions were constantly swirled for about half an hour to guarantee even mixing.

Glass substrates were ultrasonically cleaned for 15 minutes each using methanol, acetone, and deionised water before being allowed to air dry. A spin coater (Apex Instruments, India, Model NXG-P1) was used to apply the prepared sols to the cleaned substrates. Spin coating at 1500 rpm for 15 seconds and drying at 100°C for 5 minutes comprised each deposition cycle. To achieve consistent thin layers, the coating-drying cycle was repeated ten times. In order to enhance crystallinity and eliminate any remaining organic species, the deposited films were lastly annealed in air at 500°C for two hours.

2.2. Techniques for Material Characterisation:

X-ray diffraction (XRD) using Cu Kα radiation was used to analyse the crystalline structure of the deposited thin films. The Debye-Scherrer equation was used to estimate the average crystallite size. Atomic force microscopy (AFM) was used to characterise the surface topography, while field-emission scanning electron microscopy (FESEM) was used to examine surface morphology and layer thickness. A UV-visible spectrophotometer was used to assess the films' optical characteristics, and the Tauc relation was used to calculate the optical band gap.

A two-point probe arrangement was used to test the current–voltage (I–V) properties of the deposited films at ambient temperature across an applied voltage range of −20 to +20 V. Using the appropriate film dimensions and the measured electrical resistance, the films' electrical resistivity and conductivity were computed.

2.3. Gas sensor fabrication:

To create electrical contacts for sensing measures, silver paste was placed to the film's surface. The sensors were conditioned at 300°C for an entire night before testing in order to eliminate adsorbed moisture and volatile surface species. A specially constructed sensor chamber with gas inlet and outflow ports and a PID-controlled temperature controller was used for the gas-sensing measurements (shown in figure 1). All sensing experiments were conducted with a constant bias voltage of 10 V and an operating temperature of 30°C. A digital picoammeter was used to constantly monitor the proportional change in electrical resistance as ethanol vapour concentrations ranging from 100 to 500 ppm were injected into the sensing chamber.

$$S = \frac{R_{air}}{R_{gas}} \qquad (1)$$

Where R_{air} is the resistance in the presence of air and R_{gas} is the resistance in the presence of ethanol vapors. Prior to the next gas exposure, the chamber was filled with air after each sensing cycle until the sensor resistance reached its initial baseline.

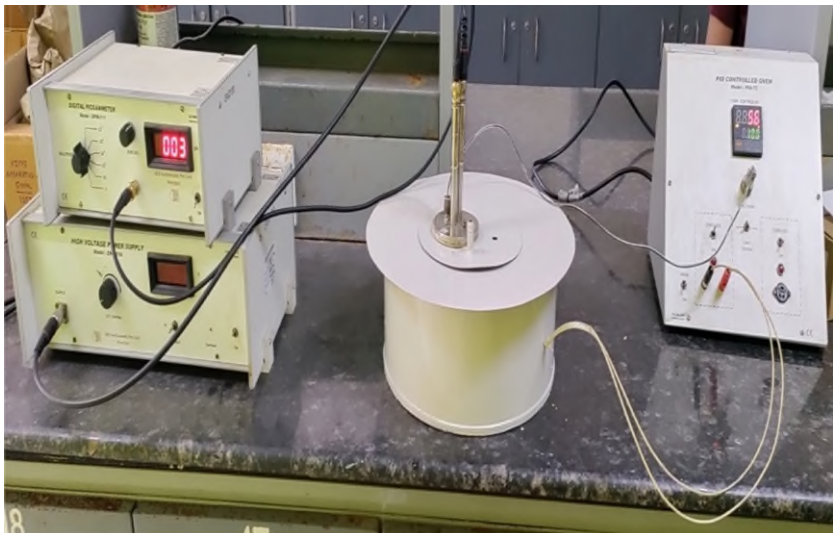


Figure 1 Experimental setup of gas sensor for the detection of ethanol gas.

After a year of storage, the optimised 0.5 at% Fe-doped TiO_2 thin film's long-term stability was assessed by monitoring its sensing response to ethanol at various concentrations. Five successive sensing cycles toward 500 ppm ethanol under the same operational circumstances were recorded in order to evaluate repeatability.

By monitoring the reaction to 500 ppm ethanol at relative humidity levels of 40%, 50%, and 60%, the impact of ambient humidity on sensor performance was examined. Additionally, the optimised

sensor's discrimination ability was assessed by subjecting it to ethanol and several interfering gases under the same experimental settings.

3. Result and discussion:

3.1. Structural and morphological studies:

The structural properties of the pure and Fe-doped TiO_2 thin films were studied by X-ray diffraction (XRD), and the matching diffraction patterns are displayed in Figure 2. All diffraction peaks may be indexed to the tetragonal anatase phase of TiO_2, with characteristic reflections corresponding to the (101), (004), (200), (105), (211), and (204) crystallographic planes situated at roughly 25°, 38°, 48°, 54°, 55°, and 63°, respectively. The detected diffraction peaks are in good agreement with the standard ICDD/JCPDS card No. 21-1272, showing the successful production of the anatase TiO_2 phase. Furthermore, no new diffraction peaks related to crystalline iron oxides or other impurity phases were found within the detection range of the XRD instrument, showing that Fe inclusion did not modify the crystal structure of anatase TiO_2. Using the classical Scherrer equation, the average crystallite size of the thin films was calculated from the highest-intensity (101) orientation peak in order to assess the impact of iron inclusion on lattice crystallinity [16]:

$$D = \frac{0.9 \times \lambda}{\beta \times \cos\theta} \qquad (2)$$

Where D is the crystallite size in nm, λ is X-rays wavelength (CuKα), β is the full width half maxima (FWHM), θ is the diffraction angle. Table 1 provides a summary of the computed structural parameters. For pure TiO_2, the average crystallite size was 17.62 nm; for the 0.5, 1.0, and 1.5 at.% Fe-doped films, it was 22.80 nm, 23.16 nm, and 26.79 nm, respectively; for the 2 at.% Fe-doped film, it was 20.46 nm. The interplanar spacing and lattice parameters showed a similar pattern, with relatively minor changes as the content of Fe increased. These findings suggest that Fe inclusion maintains the anatase crystal structure while affecting the crystal growth behaviour [15]. The reduction of crystallite formation at higher dopant concentrations may be the cause of the observed decrease in crystallite size for the 2 at.% Fe-doped TiO_2 thin film. As documented by previous studies, excess transition-metal dopants can preferentially segregate toward grain boundaries during thermal annealing, resulting in a grain-boundary pinning effect that restricts grain-boundary movement and prevents further crystallite formation. This trend is consistent with the decrease in crystallite size shown in the current work and has been extensively documented for transition-metal-doped TiO_2 systems [26,27].

The d-spacing and lattice parameters of the TiO_2 thin films were estimated by using relation:

$$d_{hkl} = \frac{n\lambda}{2\sin\theta_{hkl}} \qquad (3)$$

$$\frac{1}{d_{hkl}^2} = \frac{h^2 + k^2}{a^2} + \frac{l^2}{c^2} \qquad (4)$$

Where hkl are the miller indices, a and c are the lattice parameters and d is lattice spacing.

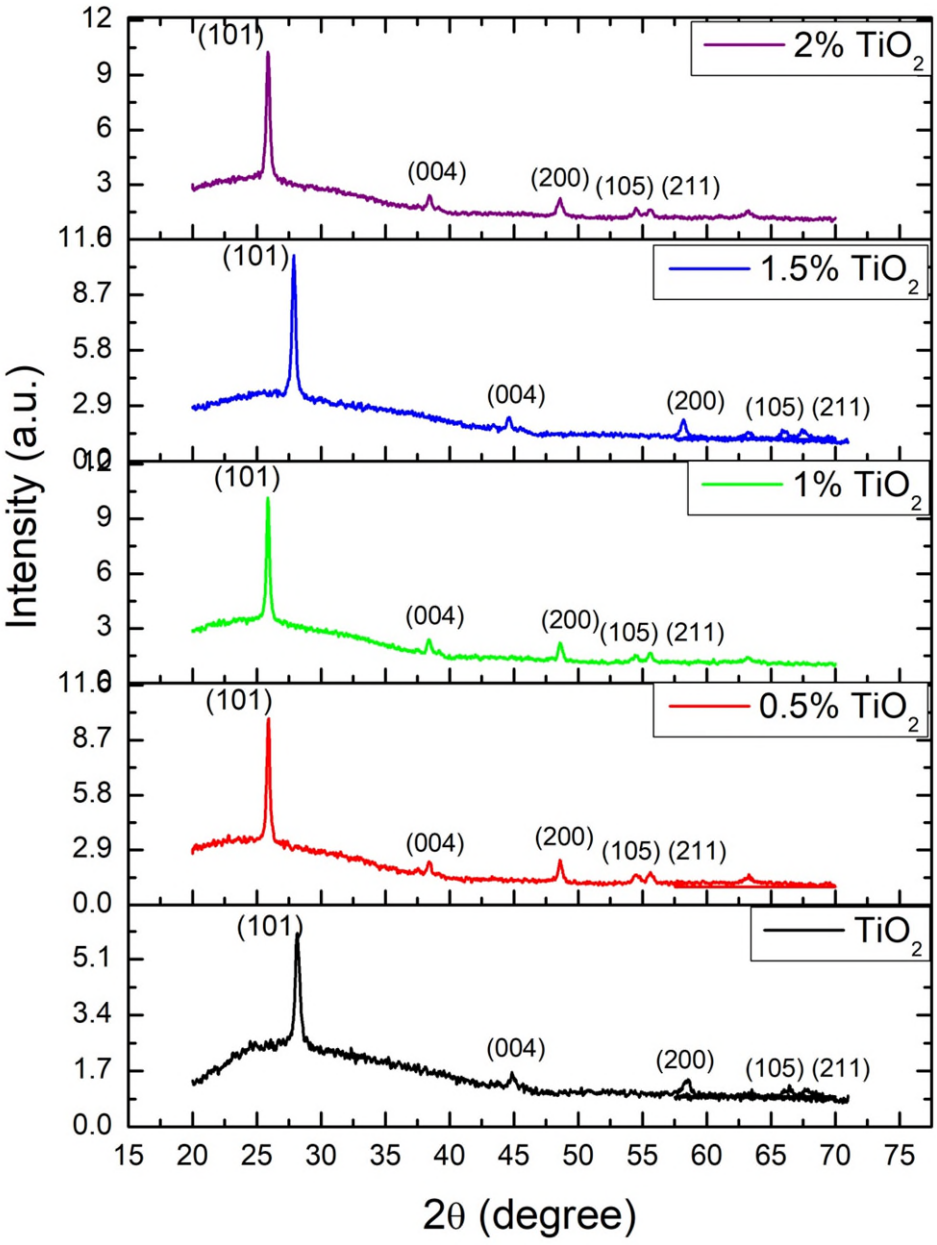


Figure 2 XRD patterns of the pure and Fe doped Titanium dioxide thin films.

The lattice parameters a and c for the pure and Fe-TiO_2 thin films are presented in table 1. The estimated lattice parameters reveal only minimal alterations with increasing Fe concentration, indicating that the anatase framework remains mostly intact following Fe incorporation [28].

Higher Fe concentrations may also limit crystallite formation, which could change the availability of active adsorption sites and decrease the efficiency of charge transport over the sensing layer. Consequently, despite the ongoing presence of the anatase phase, excessive Fe incorporation does not further increase the ethanol-sensing response, showing the existence of an optimum dopant concentration for achieving balanced structural and sensing features.

Table 1 Crystallite size of the pure and Fe doped titanium dioxide thin films.

Fe Doping (Conc.)	**FWHM (radians) (101)**	**d-spacing (Å)**	**Lattice Parameters**		**Cryatllite size d (nm)**
			a = b (Å)	**c (Å)**	
0%	0.0086	3.41141	3.721	9.31206	17.62 nm
0.5%	0.0062	3.43558	3.74493	9.36573	22.80 nm
1%	0.0061	3.43593	3.74493	9.37054	23.16 nm
1.5%	0.0056	3.43625	3.74123	9.35435	26.79 nm
2%	0.0074	3.44093	3.74345	9.36573	20.46 nm

The crystal structure and local lattice disorder of pure and Fe-doped TiO_2 thin films were examined using Raman spectroscopy, as seen in figure 3. Four distinctive Raman-active modes, which are attributed to the Eg(1), B1g, A1g + B1g, and Eg(2) vibrational modes of anatase TiO_2, are present in all samples and are centred at roughly 143, 397, 515, and 639 cm^{-1}. The dominant Eg(1) mode, which is commonly identified as the fingerprint of the anatase phase, is detected about 143 cm^{-1} and corresponds to the symmetric bending vibration of the O–Ti–O bonds. These distinctive bands are present in all compositions, indicating that the anatase framework is maintained across the studied doping range and confirming that Fe inclusion does not change the crystal symmetry of TiO_2. Additionally, no other Raman bands linked to brookite TiO_2, rutile TiO_2 (≈447 and 612 cm^{-1}), or iron oxide phases like Fe_2O_3, Fe_3O_4, and $FeTiO_3$ are seen, suggesting that Fe is integrated into the TiO_2

lattice without creating observable secondary phases. These findings are consistent with prior studies that demonstrate that substitutional Fe incorporation at low concentrations suppresses unwanted phase segregation while maintaining the anatase structure [29]. A close inspection of the spectra shows that, as the concentration of Fe increases, the dominant Eg(1) mode's strength gradually decreases along with a small peak broadening, while the Raman peak positions essentially stay the same. Such spectral evolution is frequently linked to the replacement of Fe^{3+} for Ti^{+}, which results in local lattice distortion due to the change in valence state and ionic radius. Oxygen vacancies and Ti^{3+} defect states are created to compensate for the ensuing charge imbalance, resulting in short-range structural disorder while preserving the long-range anatase crystal structure. Thus, the observed broadening and decreased intensity of the distinctive anatase modes result from relaxation of the Raman selection rules. Similarly, recent research has shown that at moderate dopant concentrations, Fe insertion alters the local Ti–O bonding environment, broadens the Eg Raman mode, and raises the number of oxygen vacancies without causing phase shift [30,31]. For ethanol gas detection, the formation of lattice defects and the maintenance of the anatase phase are very beneficial. Oxygen vacancies increase the concentration of chemisorbed oxygen ions and improve the regulation of the electron depletion layer by acting as preferential adsorption sites for ambient oxygen species and facilitating electron transfer during surface redox processes. By controlling charge-carrier concentration, surface potential, and defect chemistry—all of which enhance sensing performance—metal-ion doping also increases surface reactivity. Consequently, the XRD analysis and Raman results verify the effective substitutional incorporation of Fe into the TiO_2 lattice while maintaining the anatase crystal structure and concurrently producing oxygen-vacancy-related defects that are anticipated to improve the prepared thin films' ethanol sensing properties [32].

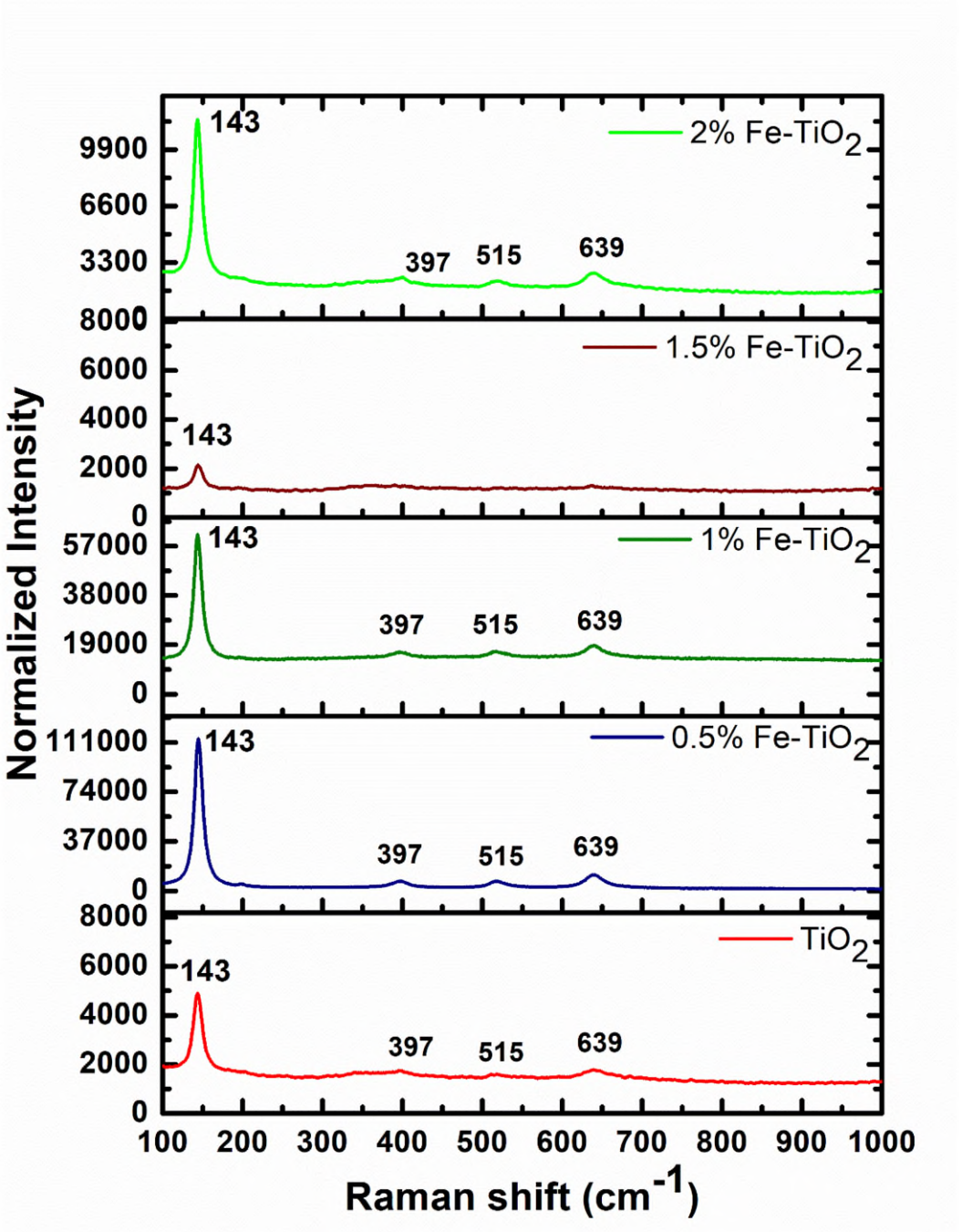


Figure 3 Raman spectra of undoped and Fe doped TiO_2 thin fims

Field-emission scanning electron microscopy (FESEM) was used to analyse the surface morphology of the deposited thin films; the resulting micrographs are displayed in Figure 4. The almost spherical nanoparticles that make up the pure TiO_2 thin film are joined to create a continuous granular network. Following Fe inclusion, the substrate surface is covered by uniformly distributed nanoparticles that maintain a comparable shape. There are no noticeable fissures or large-scale agglomerates, suggesting that continuous and uniform thin layers have formed. In close agreement with the crystallite-size trend

found in the XRD study, the average particle size measured by FESEM increased from roughly 17.62 nm for pure TiO_2 to 20–27 nm for the Fe-doped films. While there is a little decrease in particle size for the 2% at, the rise in particle size with Fe addition up to 1.5 at.% indicates improved grain growth throughout the annealing process. The lower crystallite size seen from XRD is consistent with the % Fe-doped film, suggesting that higher Fe concentrations may limit additional grain growth. All of the deposited films have a comparatively porous and interconnected microstructure, according to the FESEM pictures. Because it allows ethanol molecules to diffuse across the sensing layer and offers a large accessible surface area for gas adsorption, such a porous morphology is beneficial for gas-sensing applications. Furthermore, upon gas exposure, the linked nanoparticles create continuous conduction channels that are advantageous for charge transport [33]. The 0.5 at.% Fe-doped TiO_2 thin film showed the highest ethanol sensing response, despite the crystallite size constantly increasing up to 1.5 at.% Fe inclusion. This suggests that crystallite size is not the only factor influencing sensing performance. Rather, a combination of crystallinity, particle connectedness, electrical conductivity, and the presence of active surface adsorption sites is probably responsible for the increased reaction. While additional increases in dopant concentration may negatively affect the sensing capabilities despite the increased crystallite size, moderate Fe incorporation seems to offer the best compromise between these parameters [26,34]. Therefore, rather than a single microstructural feature, the 0.5 at.% Fe-doped TiO_2 thin film's better sensing performance can be attributed to the beneficial combination of its structural and morphological characteristics

The creation of a continuous, compact thin layer with an average thickness of around 360 nm is confirmed by the cross-sectional FESEM image. It is anticipated that the film's consistent thickness and strong adherence to the substrate will offer steady electrical conduction routes and enhance the sensing response's repeatability [35].

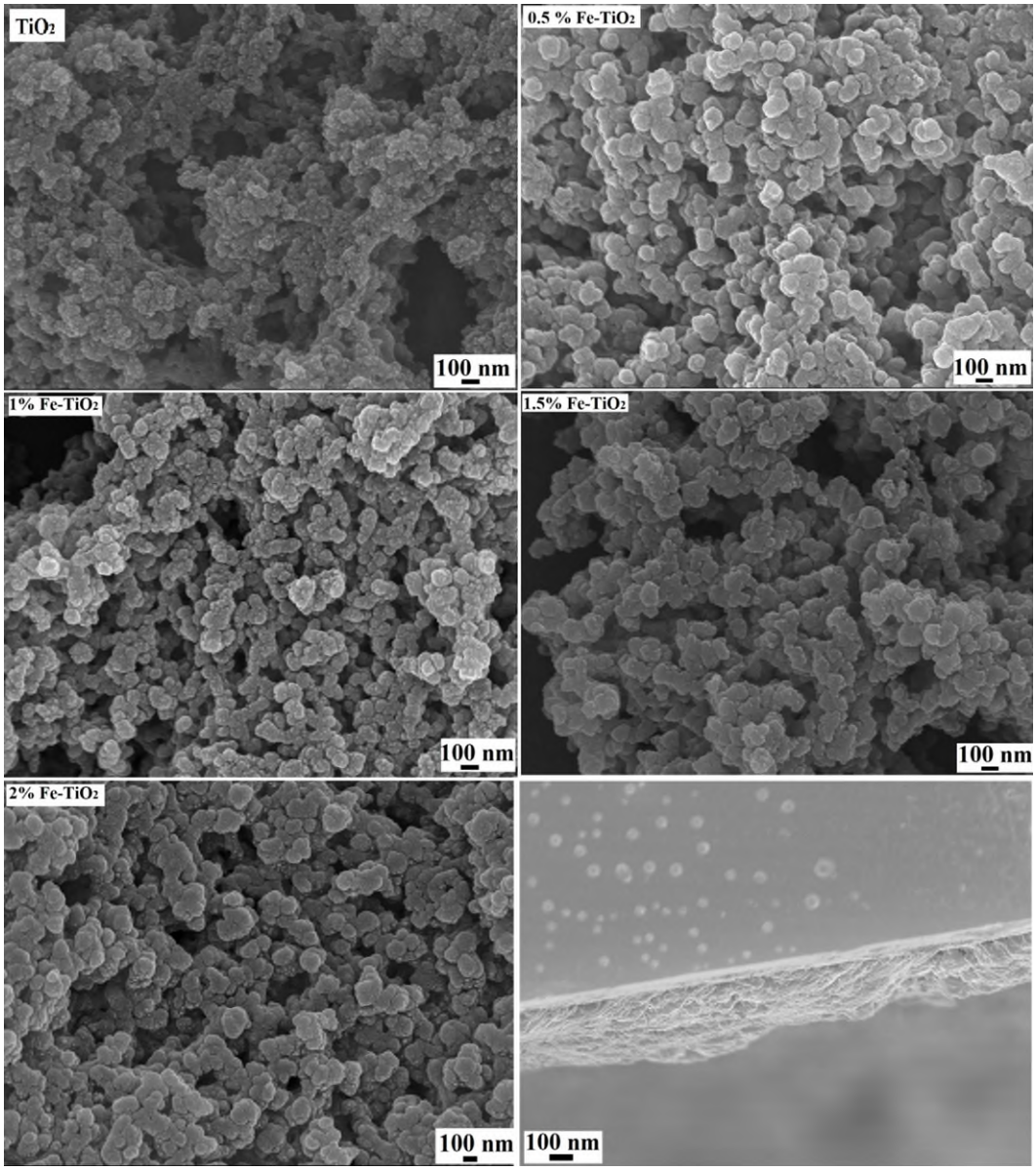


Figure 4 FESEM micrographs of pure TiO_2 and Fe-TiO_2 thin films.

3.2 Electrical studies:

A two-point probe arrangement was used to methodically examine the electrical transport characteristics of the pristine and Fe-doped TiO_2 thin films. The comparative current-voltage (I-V) profiles captured during a symmetric bipolar voltage sweep from -20 V to +20 V are shown in Figure 5. With respect to the applied bias, the current dependency of both the undoped and iron-modified TiO_2 matrices is extremely linear and symmetric. Excellent ohmic behaviour is confirmed by this perfect linearity, which shows that the well-established silver-paste electrodes offer stable electrical interfaces with minimal contact resistance. In order to remove interfacial parasitic signals and guarantee that future gas-sensing and charge-transport measurements accurately reflect the inherent electrical properties of the thin films, it is essential to secure such non-rectifying connections.

Additionally, consistent, stable charge transport across the film network is indicated by the complete lack of structural hysteresis or nonlinear trends throughout the voltage window—a crucial characteristic for attaining excellent operational repeatability and reducing baseline drift during sensor operation.

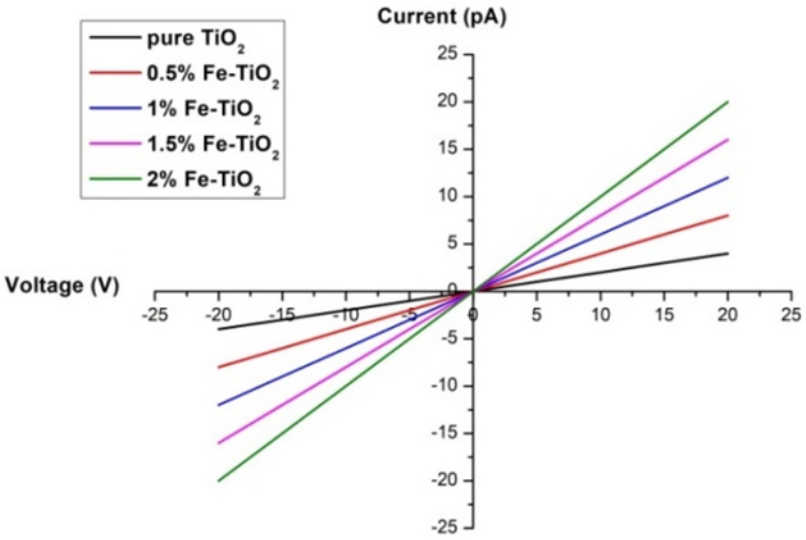


Figure 5 I-V plot of the pure and Fe doped titanium dioxide thin films at room temperature (30 ℃).

Using the relation given below the resistivity and conductivity of thin films were calculated [36]:

$$\rho = R\,\frac{A}{l} \qquad (3)$$

$$R = \frac{V}{I} \qquad (4)$$

Where ρ is the resistivity, R is the resistance, A is the area of the films, and l is the thickness of the films. V is the voltage applied and I is the current.

Table 2 displays the electrical transport characteristics of both pure and Fe-doped TiO_2 thin films. The resistivity gradually drops from 7.4×10^{11} Ω cm for pure TiO_2 to 3.8×10^{11} Ω cm for the 2 at.% Fe-doped film, while the corresponding conductivity rises from 1.36×10^{-11} to 2.62×10^{-11} S cm^{-1}. This improvement is explained by the substitution of Fe^{3+} for Ti^{+}, which raises the concentration of charge carriers and creates oxygen vacancies for charge compensation. By lowering the grain-boundary potential barrier and minimising carrier dispersion, these imperfections promote electron transport and increase electrical conductivity. Similar behaviour has been seen for Fe-doped TiO_2, where oxygen-vacancy production and substitutional Fe incorporation greatly enhance electrical transport

characteristics [13,32,37]. The 0.5 at.% Fe-doped sample demonstrates better ethanol sensing performance even though the 2 at.% Fe-doped film has the highest conductivity, suggesting that an ideal balance between electrical conductivity and surface-active defect sites is more important than maximal conductivity alone [31,38].

Table 2 The calculated resistivity and conductivity of the thin films

Fe conc.	**Resistivity (10^{14}) (Ωcm)**	**Conductivity (10^{-15}) (S cm^{-1})**
0	7.4	1.36
0.5%	5.6	1.7
1%	5.3	1.86
1.5%	4.8	2.0
2%	3.8	2.62

3.3 Ethanol sensing studies:

Figure 6(a–e) shows the dynamic ethanol detecting properties of pure and Fe-doped TiO_2 thin films toward ethanol concentrations between 100 and 500 ppm, and Figure 6 summarises the corresponding sensor response. All sensors show a sharp drop in electrical resistance when exposed to ethanol, which is consistent with the normal behaviour of an n-type semiconductor in which ethanol combines with chemisorbed oxygen species and releases electrons back into the TiO_2 conduction band. The resistance quickly returns to its starting value after the ethanol is removed, exhibiting strong reversibility and repeatability over subsequent sensing cycles. Of all the samples examined, the 0.5 at.With a sensor response that rises from roughly 4.2 at 100 ppm to 19.54 at 500 ppm—more than three times higher than that of pure TiO_2 (≈6 at 500 ppm), 0.5 at.% Fe-doped TiO_2 thin film demonstrates the best sensing performance. The optimal assimilation of Fe^{3+} ions into the TiO_2 lattice, which encourages the creation of oxygen vacancies and surface defect states, is responsible for this extraordinary increase. By serving as active adsorption sites for ambient oxygen, these oxygen vacancies raise the concentration of chemisorbed oxygen species (O_2^-, O^-) that take part in the oxidation of ethanol molecules. As a result, during ethanol oxidation, more electrons are liberated back into the conduction band, leading to a greater modulation of the depletion layer and a markedly improved sensor response. Ren et al. and Kumarage et al. have demonstrated similar gains in ethanol sensing as a result of Fe-induced oxygen vacancies [32,34]. Although the electrical conductivity

continuously improves with increasing Fe concentration, the sensing response diminishes beyond 0.5 at.% Fe, with the 1%, 1.5%, and 2% Fe-doped films exhibiting increasingly lower responses. This behaviour shows that excessive Fe incorporation produces an excessive concentration of structural defects, leading to defect clustering, grain-boundary segregation, and increased electron–hole recombination [36,37]. Moreover, the increased intrinsic conductivity reduces the breadth of the electron depletion layer, hence minimising the relative resistance modulation produced during ethanol adsorption. As a result, fewer active adsorption sites effectively participate in the surface reaction despite the larger carrier concentration [33,38]. Similar observations have been observed for Fe-doped TiO_2 and other doped metal oxide gas sensors, where intermediate dopant concentrations improve sensing performance, while excessive doping deteriorates sensitivity due to increased recombination and lower surface reactivity [38].

The 0.5 at.% Fe-doped TiO_2 thin film shows considerably better sensing kinetics in addition to having the highest sensing response. Compared to the pure TiO_2 sensor, the sensor's response time of 60 s and recovery time of 90 s are significantly shorter. In contrast, the recovery time varies between 100 and 156 seconds, while the reaction time of pure TiO_2 drops from 180 seconds at 100 ppm to 120 seconds at 500 ppm. The higher concentration of oxygen vacancies and active surface sites produced by substitutional Fe^{3+} incorporation, which promote quick oxygen chemisorption and quicken the oxidation of ethanol molecules, are responsible for the Fe-doped sensor's quicker response and recovery. Additionally, the enhanced electrical conductivity and porous microstructure promote gas diffusion and electron transport, leading to faster adsorption–desorption kinetics and better sensing performance [33,34,39].

The structural, Raman, FESEM, and electrical studies all support the improved sensing behaviour of the 0.5 at.% Fe-doped TiO_2 thin film. Raman spectroscopy shows oxygen-vacancy-induced lattice disorder without secondary phase formation, FESEM shows a porous microstructure favourable for gas diffusion, electrical measurements show adequate carrier transport while preserving an effective depletion layer, and XRD verifies the preservation of the anatase phase. The maximum ethanol sensing response for the 0.5 at is produced by the synergistic interplay of these structural and electrical features.Fe-doped thin-film TiO_2.

Mechanism for Gas Sensing

By absorbing conduction-band electrons, oxygen molecules in air are adsorbed on the TiO_2 surface to create chemisorbed oxygen species, according to

$$O_{2ad} + e^- \leftrightarrow O_2^- \qquad T < 100^oC \qquad (6)$$

The adsorbed oxygen species oxidise ethanol when it comes into contact with it.

$$C_2H_5OH + 3O_2^- (ads) \rightarrow 2CO_2 + 3H_2O + 3e^- \quad T < 100°C \qquad (7)$$

By returning to the TiO_2 conduction band, the liberated electrons lower the n-type semiconductor's resistance. By boosting oxygen-vacancy concentration and promoting oxygen adsorption, Fe doping improves this process, resulting in a greater resistance change and stronger sensing response [40].

The Kröger–Vink reaction compensates for the charge imbalance caused by the substitution of Fe^{3+} ions for Ti^{+} lattice positions by creating oxygen vacancies [41]:

$$Fe^{3+} \xrightarrow{TiO_2} Fe_{Ti} + V_{\ddot{O}} + O_O^* \qquad (7)$$

At the ideal Fe concentration, the produced oxygen vacancies improve electrical conductivity and ethanol sensing capability by increasing the concentration of surface-active defect sites and facilitating electron transport. A schematic representation of the suggested sensing mechanism is shown in Figure 7 to clarify the improved ethanol sensing performance of the Fe-doped TiO_2 thin films. The mechanism is based on the existing adsorption–desorption model reported for TiO_2-based metal oxide semiconductor gas sensors, as well as the structural, electrical, and gas-sensing results found in this study.

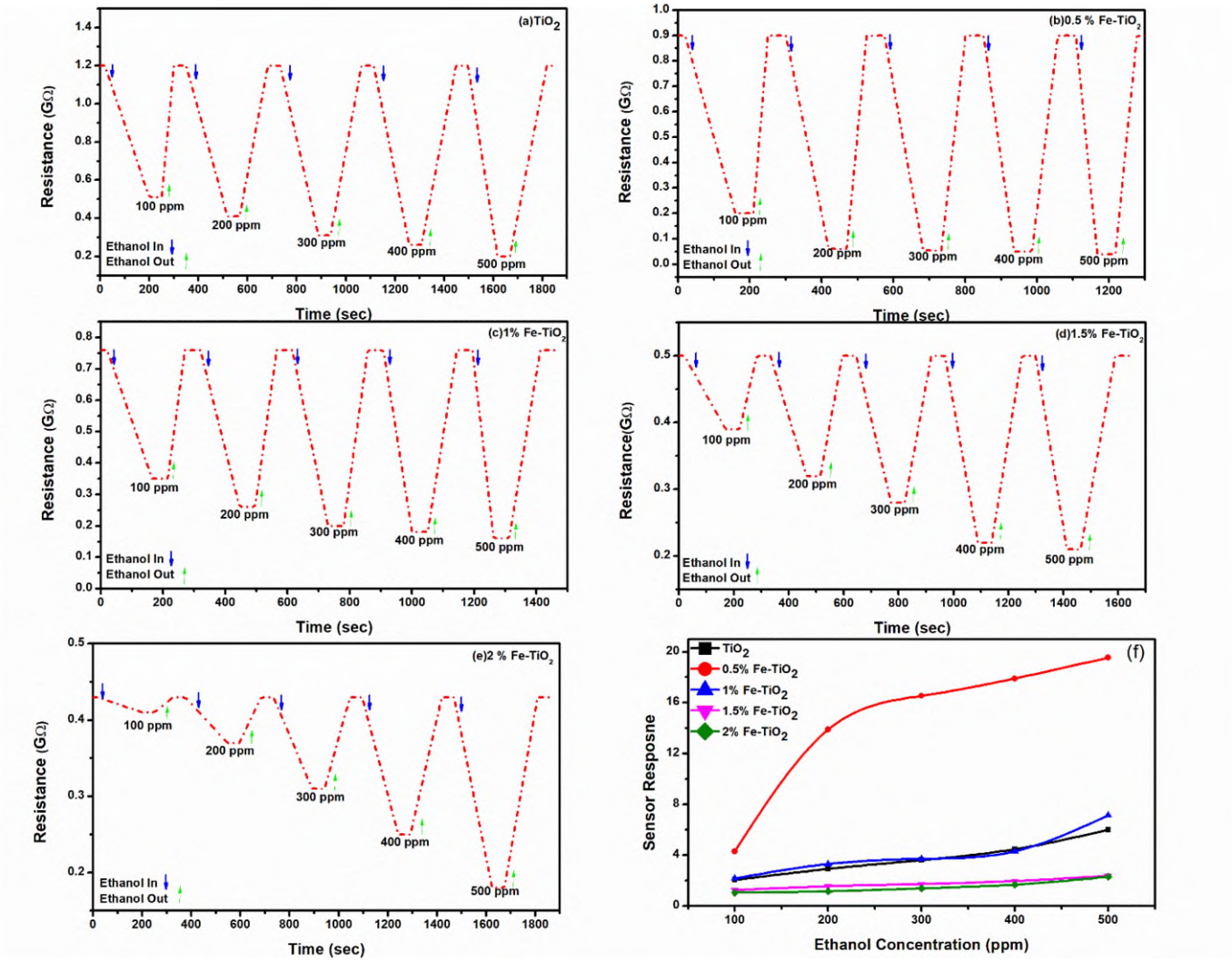


Figure 6 Response transient curve of pure and Fe doped TiO_2 thin films and sensor response of the pure and Fe doped TiO_2 thin films as a function of ethanol gas concentration at room temperature (30℃).

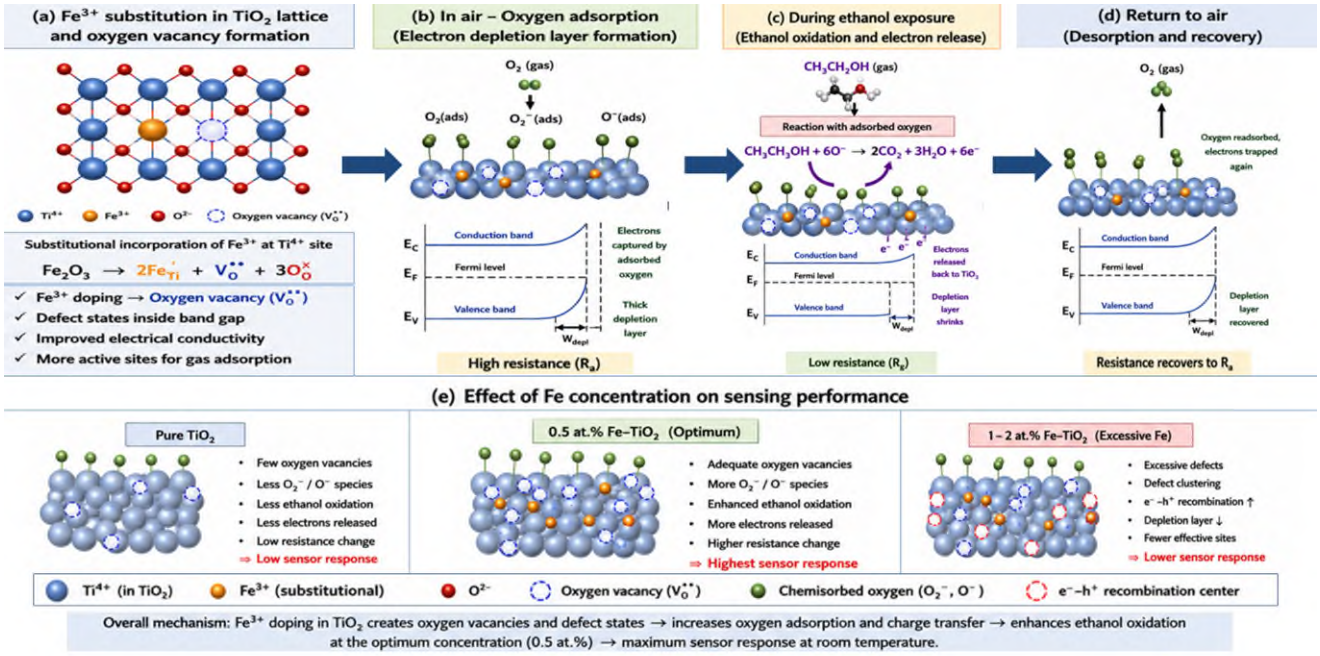


Figure 7 Proposed ethanol sensing mechanism of Fe-doped TiO_2 thin films illustrating (a) substitutional incorporation of Fe^{3+} and oxygen-vacancy formation, (b) oxygen adsorption and electron depletion layer formation in air, (c) ethanol oxidation and electron release during gas exposure, (d) recovery after ethanol removal, and (e) the influence of Fe concentration on sensing performance.

The ethanol sensing capabilities of the current Fe-doped TiO_2 thin films and previously published TiO_2-based ethanol sensors are contrasted in Table 3. The 0.5 at.% Fe-doped TiO_2 sensor created in this work has a response of 19.54 toward 500 ppm ethanol at ambient temperature. The current sensor exhibits competitive sensing capability at room temperature without the need for external heating when compared to previously published TiO_2-based sensors. The higher electrical conductivity, oxygen-vacancy production, substitutional Fe inclusion, and the porous microstructure all work in concert to promote effective adsorption and charge transfer during ethanol sensing, which is responsible for the improved performance.

Table 3 Comparative ethanol sensing characteristics of TiO_2 thin films.

TiO_2 thin films	**Technique Used**	**Ethanol Concentration**	**Operating Temperature**	**Sensor Response**	**Ref.**
Cr-TiO_2 thin films	Rf Sputtering	10-100 ppm	300° C	35 (100 ppm)	[42]

TiO_2 thin films	CVD	12 Pa	200° C	37	[43]
Pt/Nb doped TiO_2 thin films	Sol-gel spin coating	500 ppm	300° C - 500° C	2370% (500° C)	[35]
Pt/Nb doped TiO_2 thin films	Sol-gel spin coating	125-500 ppm	290° C - 400° C	41 for 1000 ppm (380° C)	[44]
TiO_2 thin films	DC magnetron sputtering	-	150° C - 350° C	3.5 (275° C)	[45]
W-TiO_2 thin films	Sol-gel spin coating technique	100-500 ppm	300° C - 500° C	1230% for 500 ppm (350° C)	[46]
Fe/TiO_2 thin films	Micro-arc oxidation	1000 ppm	200-300° C	7.91 at 275° C	[34]
Phase-engineered TiO_2	RF Magnetron Sputtering	50-600 ppm	250°C	14.20 for 500 ppm	[26]
Donor-doped TiO_2	Sol-Gel Dip Coating	50 – 500 ppm	Room temperature (with light)	4.50 for 500 ppm	[15]
Fe-TiO_2 thin films	Sol-gel spin coating	100-500 ppm	Room temperature	19.54	Our Work

3.4. Repeatability and Long-Term Stability:

After a year of storage, the optimised 0.5 at% Fe–TiO_2 thin-film sensor's long-term stability and repeatability were assessed, as seen in Figure 8(a–b). Excellent structural stability and resistance to baseline drift are demonstrated by the dynamic sensing responses toward 100, 300, and 500 ppm ethanol (Figure 8(a)), which show minimal degradation in both response magnitude and sensing kinetics after the ageing period. The sensor confirms the reversible nature of the adsorption–

desorption process by maintaining a rapid drop in resistance upon exposure to ethanol and recovering almost to its initial baseline following ethanol removal.

As shown in Figure 8(b), cyclic repeatability experiments were carried out utilising five successive exposure–purging cycles under 500 ppm ethanol to further assess the operational reliability. Excellent consistency and reproducibility of the sensing behaviour are shown by the almost overlapping response curves and the constant baseline resistance and response magnitude over subsequent cycles. The Fe-doped TiO_2 sensing layer experiences reversible surface reactions without irreversible surface poisoning or structural degeneration, as evidenced by the lack of discernible signal degradation or baseline fluctuation. The stable oxygen-vacancy-related active sites, uniform Fe inclusion, and retained anatase crystal structure are responsible for the exceptional long-term stability, while the porous shape promotes effective gas diffusion and quick reaction product desorption. These findings demonstrate the optimised 0.5 at.% Fe–TiO_2 thin film's exceptional long-term operational stability and dependability, underscoring its promise for useful room-temperature ethanol sensing applications [47,48].

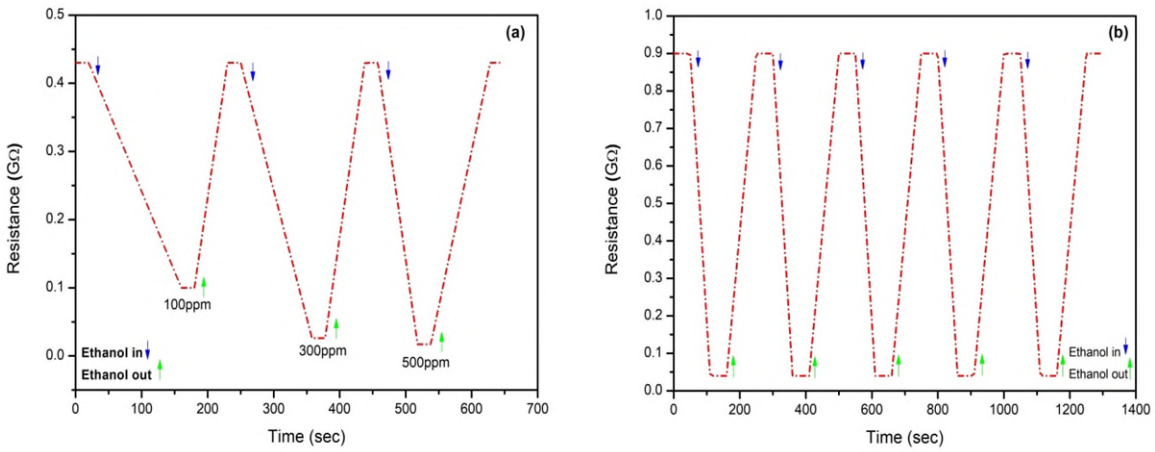


Figure 8 (a) Stability of the 0.5% Fe-TiO_2 thin film at different concentration after 1 year of storage, (b) Reproducibility of the 0.5% Fe-TiO_2 thin film repeated for five cycles towards 500 ppm of ethanol at room temperature (30℃).

3.5. Relative Humidity's Impact on Ethanol Sensing and Selectivity:

The effect of ambient humidity on the ethanol sensing performance seen in Figure 9, the 0.5 at.% Fe–TiO_2 thin film was examined at 40%, 50%, and 60% relative humidity (RH). Excellent operational stability in humid situations is demonstrated by the sensor's steady and reversible dynamic responses toward both 100 and 500 ppm ethanol under all humidity conditions. The response to 500 ppm ethanol only slightly drops, from 19.54 at 40% RH to 18.36 at 60% RH, or roughly 6%. Similarly, the

response to 100 ppm ethanol likewise only slightly varies. The response and recovery characteristics show that humidity has relatively little effect on the sensing kinetics.

The competing adsorption of water molecules and oxygen species on the active surface sites of the Fe–TiO_2 thin film is responsible for the small decrease in sensor responsiveness with rising RH. The amount of chemisorbed oxygen accessible for ethanol oxidation is decreased at higher humidity levels because adsorbed water molecules partially occupy oxygen-vacancy-related adsorption sites and generate surface hydroxyl groups. As a result, during the surface reaction, fewer electrons are liberated into the conduction band, which causes the resistance modulation to slightly decrease [49]. However, the slight reduction in sensing effectiveness suggests that the porous microstructure and Fe-induced oxygen vacancies maintain enough active sites for ethanol adsorption even in humid environments. These findings show that the optimised 0.5 at% Fe–TiO_2 thin film has good humidity endurance and may be used for accurate room-temperature ethanol sensing in real-world settings.

As seen in Fig. 10, 0.5 at% Fe–TiO_2 thin film's selectivity toward ethanol, methanol, acetone, xylene, formaldehyde, benzene, and toluene was assessed at a fixed concentration of 500 ppm. The sensor's response to ethanol is remarkably high (19.54), but its responses to methanol (1.50), acetone (1.66), xylene (1.33), formaldehyde (2.34), benzene (2.00), and toluene (1.63) are much lower. The preferential adsorption and oxidation of ethanol molecules on the Fe-induced oxygen-vacancy-rich TiO_2 surface, which leads to improved charge transfer and a greater resistance modulation, is responsible for the exceptional selectivity for ethanol. These findings show that the Fe-doped TiO_2 thin film has exceptional selectivity for accurate ethanol detection at ambient temperature, even when interfering volatile organic compounds (VOCs) are present.

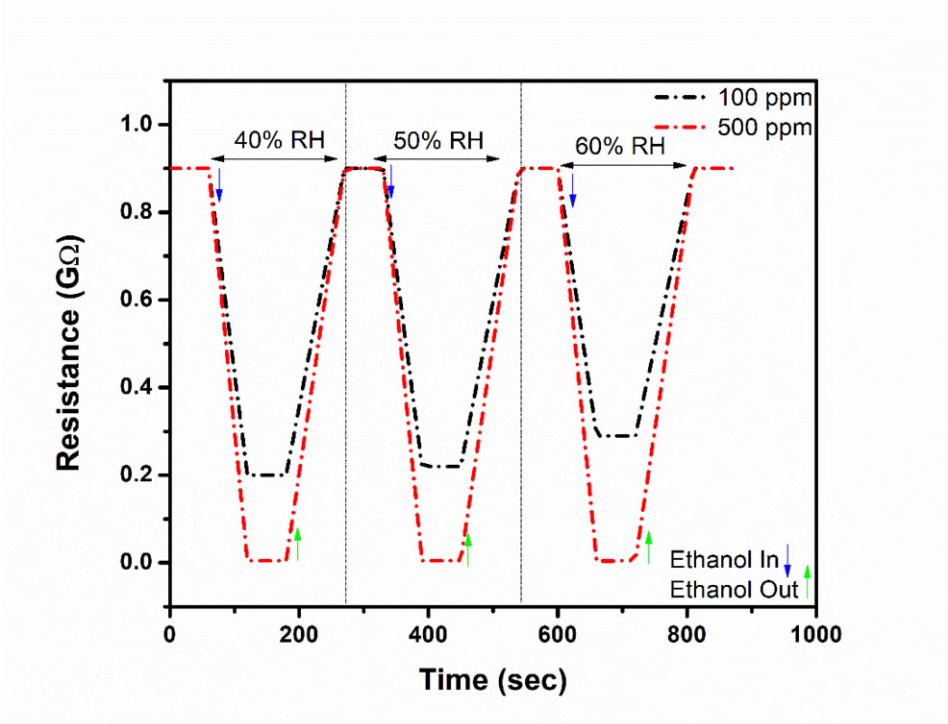


Figure 9 Response and recovery plot of sample 0.5% Fe-TiO_2 thin film for 100 and 500 ppm at different relative humidity.

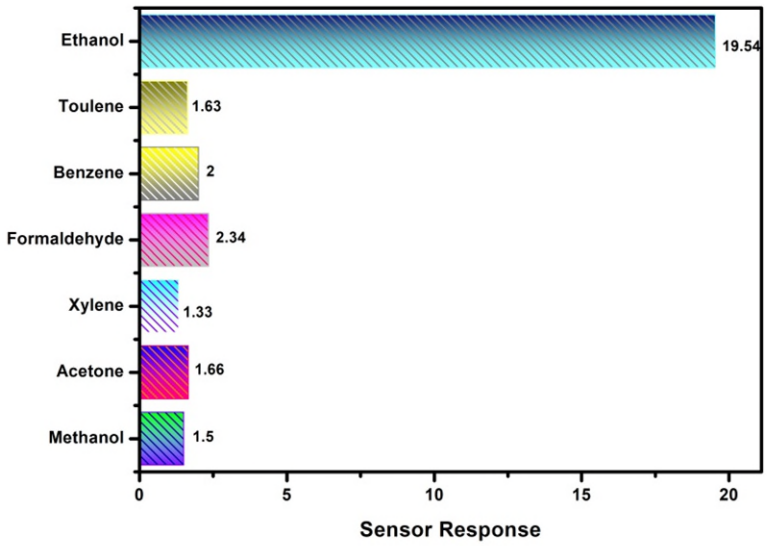


Figure 10 Selectivity of the 0.5% Fe-TiO_2 thin film at room temperature (30° C).

4. Conclusion:

Using the sol–gel spin-coating process, Fe-doped TiO_2 thin films with Fe concentrations varying from 0 to 2 at.% were effectively synthesised and tested for ethanol sensing at ambient temperature. FESEM showed a porous shape that was advantageous for gas adsorption, and structural studies

verified the creation of a single-phase anatase TiO_2 structure with successful substitutional incorporation of Fe^{3+}. By promoting charge-carrier transport, Fe doping produced oxygen vacancies and improved electrical conductivity. With a maximum response of 19.54 toward 500 ppm ethanol and quick response and recovery durations of 60 and 90 s, respectively, the 0.5 at.% Fe–TiO_2 thin film demonstrated the best sensing performance of all the compositions. Because of increased charge-carrier recombination and excessive defect generation, higher Fe concentrations decreased sensing performance but increased conductivity. Additionally, the optimised sensor showed exceptional long-term stability and repeatability after a year of storage, minimal humidity interference with just a 6% response drop at 60% RH, and high selectivity toward ethanol over other VOCs. These results show that the 0.5 at.% Fe–TiO_2 thin film is a promising material for stable, dependable, and selective room-temperature ethanol sensing applications.

References:

[1] Gai L Y, Lai R P, Dong X H, Wu X, Luan Q T, Wang J, Lin H F, Ding W H, Wu G L and Xie W F 2022 Recent advances in ethanol gas sensors based on metal oxide semiconductor heterojunctions *Rare Met.* **41** 1818–42

[2] Alsamrai O, Redel-Macias M D and Dorado M P 2025 Real-Time Intelligent Monitoring of Outdoor Air Quality in an Urban Environment Using IoT and Machine Learning Algorithms *Appl. Sci.* **15** 1–28

[3] Hua X, Zhang J, Zhang X, Yang H, Wang M, Luo Z and Wang H 2025 Characteristics and health risk assessment of VOCs from typical hot pot restaurants in Chongqing, China *Environ. Sci. Adv.* **5** 499–509

[4] Zhang G, Huang D, Ichikawa K, Iitani K, Nakajima Y and Mitsubayashi K 2026 Headset-Type Biofluorometric Gas Sensor with CMOS for Transcutaneous Ethanol from the Ear Canal *Sensors (Basel).* **26** 1–15

[5] Shankar R V, Meetei T S, Boomadevi S, Karthick P, Jeyadheepan K, Pandiyan K, Singh P K, Singh V and Karn R K 2019 Studies on thin films of TiO2 for resistance-based sensing of ethanol vapor at room temperature *Phase Transitions* **92** 782–9

[6] Mohamad Saad P S, Sutan H B, Shariffudin S S, Hashim H and Mohd Noor U 2015 TiO2 Thin Film via Sol-Gel Method: Investigation on Molarity Effect *IOP Conf. Ser. Mater. Sci. Eng.* **99**

[7] Kruse J, Wörner J, Schneider J, Dörksen H and Pein-Hackelbusch M 2024 Methods for Estimating the Detection and Quantification Limits of Key Substances in Beer Maturation with

Electronic Noses *Sensors* **24**

[8] Li B, Zhou Q, Peng S and Liao Y 2020 Recent Advances of SnO2-Based Sensors for Detecting Volatile Organic Compounds *Front. Chem.* **8** 1–6

[9] Jo S Bin, Kim H J, Ahn J H, Hwang B W, Huh J S, Ragupathy D, Lee S C and Kim J C 2020 Effects of Thin-Film Thickness on Sensing Properties of SnO 2 -Based Gas Sensors for the Detection of H 2 S Gas at ppm Levels *J. Nanosci. Nanotechnol.* **20** 7169–74

[10] Nanda A, Singh V, Jha R K, Sinha J, Avasthi S and Bhat N 2021 Growth-Temperature Dependent Unpassivated Oxygen Bonds Determine the Gas Sensing Abilities of Chemical Vapor Deposition-Grown CuO Thin Films *ACS Appl. Mater. Interfaces* **13** 21936–43

[11] Prajesh R, Goyal V, Nahid M, Saini V, Singh A K, Sharma A K, Bhargava J and Agarwal A 2020 Nickel oxide (NiO) thin film optimization by reactive sputtering for highly sensitive formaldehyde sensing *Sensors Actuators, B Chem.* **318** 128166

[12] Zhang S, Zhang H, Yao H, Wang P, Zhu M, Shi X and Xu S 2024 Recent Advances in Metal Oxide Semiconductor Heterojunctions for the Detection of Volatile Organic Compounds *Chemosensors* **12**

[13] Diebold U 2002 <(Surf.Sci.Rep.)[2003]The surface science of titanium dioxide.pdf> *Surf. Sci. Rep.* **48** 53–229

[14] Ribarsky M W 1992 Titanium dioxide *Addit. Polym.* **1992** 4

[15] Šutka R E K K V J Š 2024 Light-Induced Room-Temperature Gas Sensing by Donor-Doped Anatase TiO2 Ultrasmall Nanoparticles *ACS Appl. Eng. Mater.* **2** 649–658

[16] Damsyik N, Said M, Sahdan Z and Nayan N 2018 RSC Advances Di ff erence in structural and chemical properties of sol – gel spin coated Al doped TiO 2 , Y doped TiO 2 29686–97

[17] Astinchap B, Ghanbaripour H and Amuzgar R 2020 Multifractal study of TiO2 thin films deposited by MO-CVD method: The role of precursor amount and substrate temperature *Optik (Stuttg).* **222** 165384

[18] Patil L A, Suryawanshi D N, Pathan I G and Patil D G 2014 Nanocrystalline Pt-doped TiO 2 thin films prepared by spray pyrolysis **37** 425–32

[19] Moon J, Kemell M, Kukkola J, Punkkinen R, Hedman H P, Suominen A, Mäkilä E, Tenho M, Tuominen A and Kim H 2012 Gas sensor using anodic Tio2 thin film for monitoring hydrogen *Procedia Eng.* **47** 791–4

[20] Wang H, Chen L, Wang J, Sun Q and Zhao Y 2014 A micro oxygen sensor based on a nano sol-gel TiO2 thin film *Sensors (Switzerland)* **14** 16423–33

[21] Pozos H G, Krishna K T V, de la Luz Olvera Amador M, Kudriavtsev Y and Alvarez A M 2018 TiO2 thin film based gas sensors for CO-detection *J. Mater. Sci. Mater. Electron.* **29** 15829–37

[22] Sadia S, Raza M A and Riaz S 2026 Enhanced CO2 Gas Sensing Performance of Au/Ag-Decorated TiO2 Hetero-Nanostructured Thin Films: A Study on Structural, Optical, and Morphological Properties *ACS Omega* **11** 19619–30

[23] Rafiq R Z M M A, Nafees M I M and Hussain A R B S G 2018 Influence of Iron Doping on Structural , Optical and Magnetic Properties of - TiO 2 Nanoparticles *Electron. Mater. Lett.* **14** 587–93

[24] Ranjit K T and Viswanathan B 1997 Synthesis, characterization and photocatalytic properties of iron-doped TiO2 catalysts *J. Photochem. Photobiol. A Chem.* **108** 79–84

[25] Benyakhlef M, Bensouici F, Bououdina M, Dakhel A A, Tala-ighil R and Toubane M 2020 Surface , structural and optical properties dependence of Fe-doped TiO 2 films deposited onto soda – lime – glass *Surfaces and Interfaces* **21** 100682

[26] Faris M M and Ayal A K 2025 Electrochemical Synthesis of Fe-doped TiO2 Nanotube for Gas Sensor Application *Iraqi J. Sci.* **66** 1437–50

[27] Marami M B and Farahmandjou M 2018 Sol – Gel Synthesis of Fe-Doped TiO 2 Nanocrystals

[28] Moradi H, Eshaghi A, Hosseini S R and Ghani K 2016 Fabrication of Fe-doped TiO2 nanoparticles and investigation of photocatalytic decolorization of reactive red 198 under visible light irradiation *Ultrason. Sonochem.* **32** 314–9

[29] Strapasson G B, Arjona A S, McPeak J E, Aalling-Frederiksen O, Sapnik A F, Baun N L, Bordallo H N, Rodella C B, Zanchet D and Jensen K M Ø 2025 Oxygen Vacancy-Induced Phase Transformations of Iron-Doped Titanium Oxide Nanostructures *ACS Nano* **19** 30986–99

[30] Markose A, Das D and Ravindran P 2023 Quantitative framework development for understanding the relationship between doping and photoelectrochemical energy conversion of TiO2 *Mater. Adv.* **4** 3399–451

[31] Khan J and Han L 2023 Oxygen Vacancy in TiO 2 : Production Methods and Properties *Updat. Titan. Dioxide* 1–21

[32] Kumarage G W C, Hakkoum H and Comini E 2023 Recent Advancements in TiO2 Nanostructures: Sustainable Synthesis and Gas Sensing *Nanomaterials* **13**

[33] Al-Hashem M, Akbar S and Morris P 2019 Role of Oxygen Vacancies in Nanostructured Metal-Oxide Gas Sensors: A Review *Sensors Actuators, B Chem.* **301**

[34] Ren F, Yu X, Ling Y and Feng J 2012 Micro-arc oxidization fabrication and ethanol sensing performance of Fe-doped TiO 2 thin films **19** 461–6

[35] Comini E, Faglia G, Sberveglieri G, Li Y X, Wlodarski W and Ghantasala M K 2000 Sensitivity enhancement towards ethanol and methanol of TiO2 films doped with Pt and Nb *Sensors Actuators, B Chem.* **64** 169–74

[36] Rajeswari R, Venugopal D, Raj A D, Arumugam J, Sundaram S J and Kaviyarasu K 2020 Materials Today : Proceedings Effect of doping concentration for the properties of Fe doped TiO 2 thin films applications *Mater. Today Proc.*

[37] Hoffmann W C T R 1994 The Role of Metal Ion Dopants in Quantum-Sized TiO2: Correlation between Photoreactivity and Charge Carrier Recombination Dynamics *J. Phys. Chem.* **98** 13669–13679

[38] Korotcenkov G and Cho B K 2017 Metal oxide composites in conductometric gas sensors: Achievements and challenges *Sensors Actuators B Chem.* **244** 182–210

[39] Vijayalakshmi K and Jereil S D 2014 Enhanced ethanol sensing performance of Fe : TiO 2 nanowires and their mechanism of sensing at room temperature *Ceram. Int.* 1–7

[40] Pandeeswari R, Karn R K and Jeyaprakash B G 2014 Sensors and Actuators B : Chemical Ethanol sensing behaviour of sol – gel dip-coated TiO 2 thin films *Sensors Actuators B. Chem.* **194** 470–7

[41] Kröger F A and Vink H J 1956 Relations between the Concentrations of Imperfections in Crystalline Solids *Solid State Phys.* **3** 307–435

[42] Alessandri I, Comini E, Bontempi E, Faglia G, Depero L E and Sberveglieri G 2007 Cr-inserted TiO2 thin films for chemical gas sensors *Sensors Actuators, B Chem.* **128** 312–9

[43] Baryshnikova M V., Filatov L A, Petrov A S and Alexandrov S E 2015 CVD Deposited Titania Thin Films for Gas Sensors with Improved Operating Characteristics *Chem. Vap. Depos.* **21** 327–33

[44] Hieu N Van, Duy N Van, Huy P T and Chien N D 2008 Inclusion of SWCNTs in Nb/Pt co-

doped TiO2 thin-film sensor for ethanol vapor detection *Phys. E Low-Dimensional Syst. Nanostructures* **40** 2950–8

[45] Mardare D, Iftimie N and Luca D 2008 TiO2 thin films as sensing gas materials *J. Non. Cryst. Solids* **354** 4396–400

[46] Garzella C, Bontempi E, Depero L E and Vomiero A 2003 Novel selective ethanol sensors : W / TiO 2 thin films by sol – gel spin-coating **93** 495–502

[47] Qiang Fu K L, Li N and Dong Z 2023 Advances in the development of MOS-based sensors for detection of ethanol: A revie *Mater. Res. Bull.* **168** 112457

[48] Isaac N A, Pikaar I and Biskos G 2022 Metal oxide semiconducting nanomaterials for air quality gas sensors: operating principles, performance, and synthesis techniques *Microchim. Acta* **189**

[49] Barsan N and Weimar U 2001 Conduction model of metal oxide gas sensors *J. Electroceramics* **7** 143–67

Author Contributions:

Neha Sharma: characterization, conceptualization, writing of manuscript, using software

Rajesh Kumar: supervision, editing of manuscript.

Author's Information:

Affilation:

PG Department of Physics, Kanya Maha Vidayalaya, Jalandhar Punjab, India.

School of Chemical Engineering and Physical Sciences, Lovely Professional University, Phagwara, Punjab-144411, India

Neha Sharma, Rajesh Kumar

Corresponding Author:

Corresponding to Rajesh Kumar

Corresponding author mail id: rajesh.12236@lpu.co.in

Statements and Declarations:

Funding: The authors declare that no funds or grants were received during this work.

Competing Interest: The Authors have no competing interest to declare that are relevant to the content of this article.

Data Availabilty Statement: The authors declare that the data supporting the findings of this study are available within the paper.

Supplementary Information: Not Applicable.

Ethical approval: Not applicable.